eLIFE elifesciences.org

RESEARCH ARTICLE

Figures and figure supplements

MicroRNA-mediated control of developmental lymphangiogenesis

Hyun Min Jung *et al*

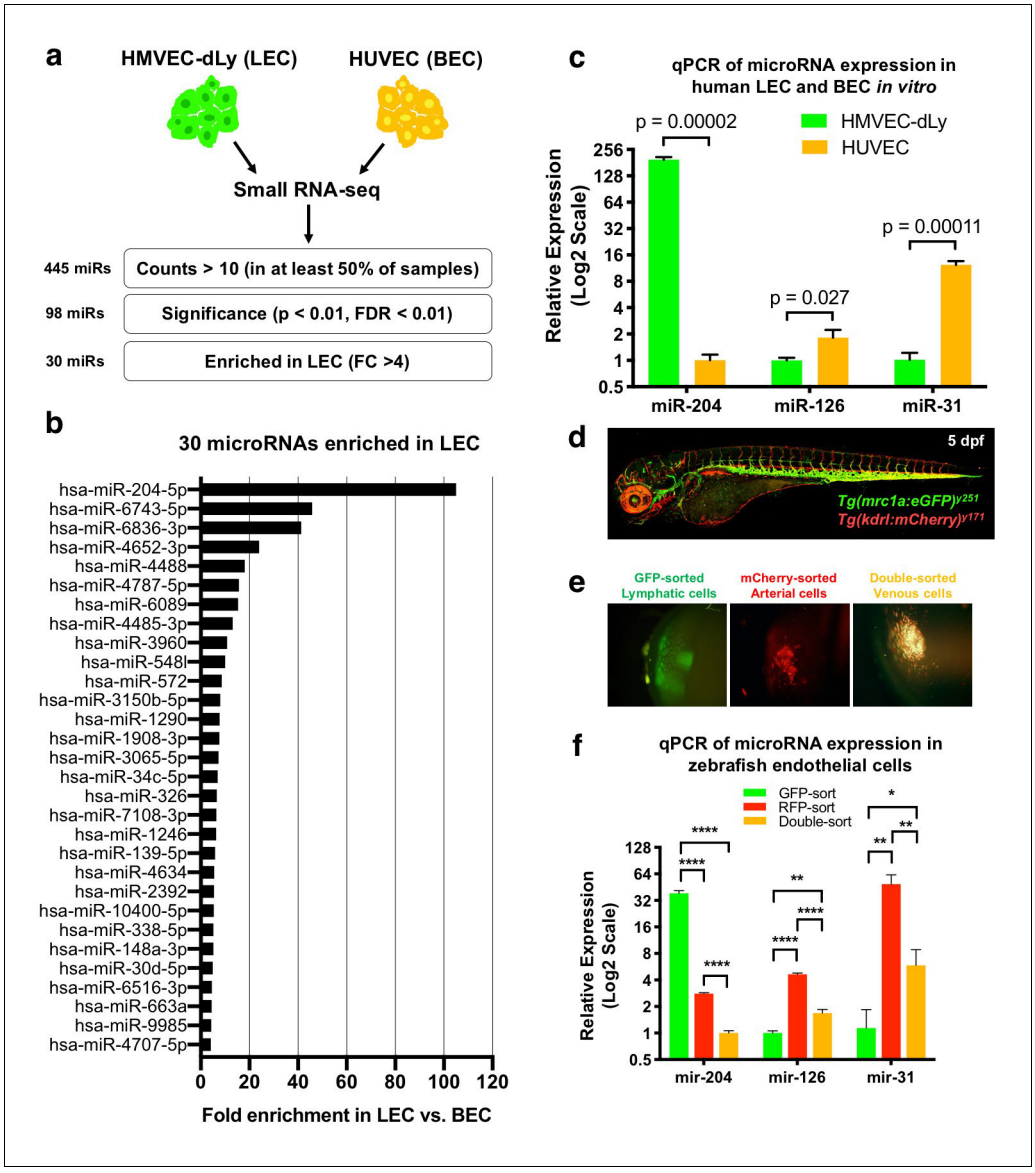

Figure 1. Identification of lymphatic microRNAs enriched in human and zebrafish lymphatic endothelial cells. (**a**) Schematic diagram of the workflow for small RNA sequencing from lymphatic (HMVEC-dLy) and blood (HUVEC) endothelial cells and selection of microRNAs enriched in lymphatic endothelial cells. (**b**) Relative fold enrichment of the 22 most highly enriched microRNAs in LEC versus BEC small RNA sequence data (average of triplicate samples from each group). (**c**) Quantitative TaqMan RT-PCR measurement of the relative expression of three different microRNAs in HMVEC-dLy (LEC) and HUVEC (BEC). Levels of mir-204 are normalized to HUVEC (BEC) levels, while levels of mir-126 and mir-31 are normalized to HMVEC-dLy (LEC) levels. Three biological replicates were analyzed. (**d**) Confocal image of a five dpf *Tg(mrc1a:eGFP)*^{y251}, *Tg(kdrl:mCherry)*^{y171} double-transgenic larva (lateral view, rostral to the left). (**e**) Confocal images of lymphatic (GFP-positive), arterial (mCherry-positive), and venous (GFP and mCherry double-positive) endothelial cell pellets isolated from dissociated five dpf transgenic animals such as that in panel d by Fluorescence Activated Cell Sorting (FACS). (**f**) Quantitative TaqMan RT-PCR measurement of the relative expression of mature mir-204, mir-126, and mir-31 in FACS-sorted zebrafish endothelial cells. FACS-sorted cells from ~1000 5 dpf larvae were used and three technical replicates were analyzed. Levels of mir-204 are normalized to venous (GFP and mCherry double-positive) levels, while levels of mir-126 and mir-31 are normalized to lymphatic (GFP-positive) levels. All graphs are analyzed by t-test and the mean ± standard deviation (SD) is shown. *, p<0.05; **, p<0.01; ****, p<0.0001.

DOI: https://doi.org/10.7554/eLife.46007.002

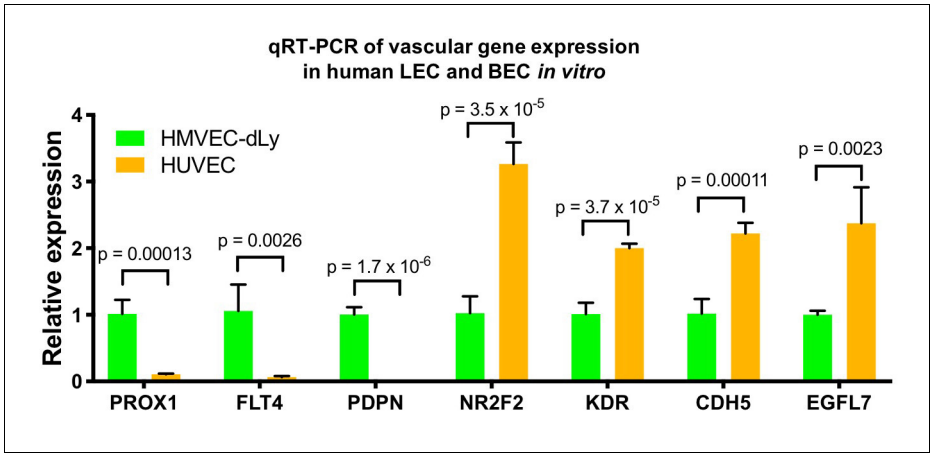

Figure 1—figure supplement 1. Differential expression of vascular genes in HMVEC-dLy and HUVEC. Quantitative TaqMan RT-PCR measurement of the relative expression of known lymphatic and blood vessel markers in HMVEC-dLy (Lymphatic Endothelial Cells, LEC) and HUVEC (Blood Endothelial Cells, BEC), normalized to expression levels in HMVEC-dLy (LEC). Four biological replicates were analyzed. All graphs are analyzed by t-test and the mean ± SD is shown.

DOI: https://doi.org/10.7554/eLife.46007.003

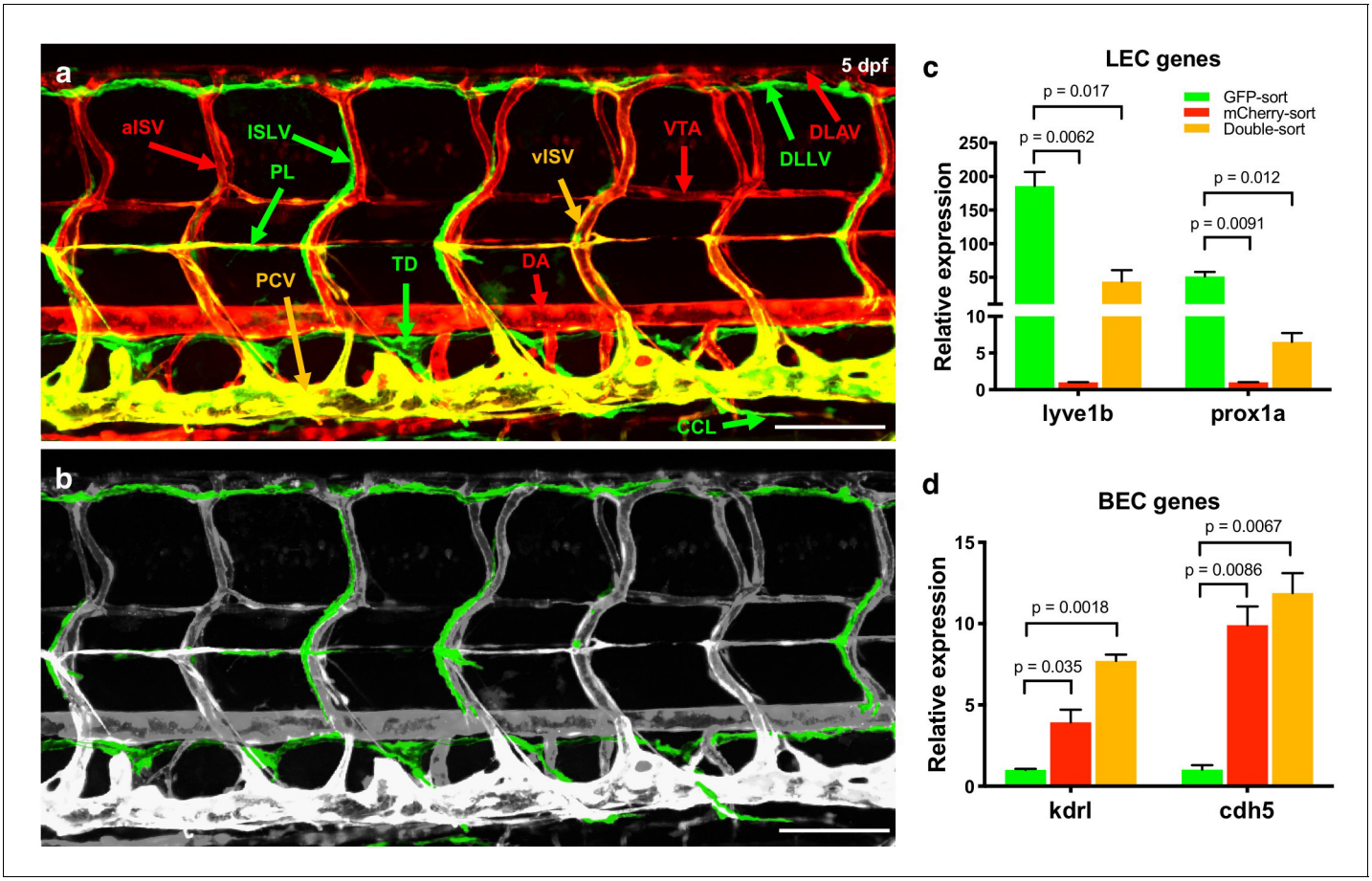

Figure 1—figure supplement 2. Trunk vascular patterning and vascular gene expression in FACS-sorted endothelial cells from transgenic zebrafish. (**a**) Confocal images of the vasculature in the mid-trunk of a five dpf *Tg(mrc1a:eGFP)*^{y251}, *Tg(kdrl:mCherry)*^{y171} double-transgenic animal with mCherry positive arterial blood vessels (red), EGFP positive lymphatic vessels (green), and mCherry and EGFP double positive venous blood vessels (yellow). The different vessels are labeled: DA, dorsal aorta; DLLV, dorsal longitudinal lymphatic vessel; DLAV, dorsal longitudinal anastomotic vessel; ISLV: intersegmental lymphatic vessel; aISV: arterial intersegmental vessel; vISV: venous intersegmental vessel; PCV, posterior cardinal vein; PL, parachordal line; TD, thoracic duct; CCL, collateral cardinal lymphatics; VTA, vertebral artery. (**b**) Confocal image from panel a with lymphatic vessels pseudocolored in green and other vessels in gray, for easier visualization of the lymphatic network. (**c**) Quantitative TaqMan RT-PCR measurement of the relative expression of lymphatic endothelial cell (LEC) genes *lyve1b* and *prox1a* in FACS-sorted zebrafish endothelial cell populations. Expression is normalized to the arterial (mCherry-positive) endothelial cell population. (**d**) Quantitative TaqMan RT-PCR measurement of the relative expression of blood endothelial cell (BEC) genes *kdrl* and *cdh5* in FACS-sorted zebrafish endothelial cell populations. Expression is normalized to the lymphatic (EGFP-positive) endothelial cell population. Scale bars = 100 μm (a,b). Biological duplicates were analyzed. All graphs are analyzed by t-test and the mean ± SD is shown.

DOI: https://doi.org/10.7554/eLife.46007.004

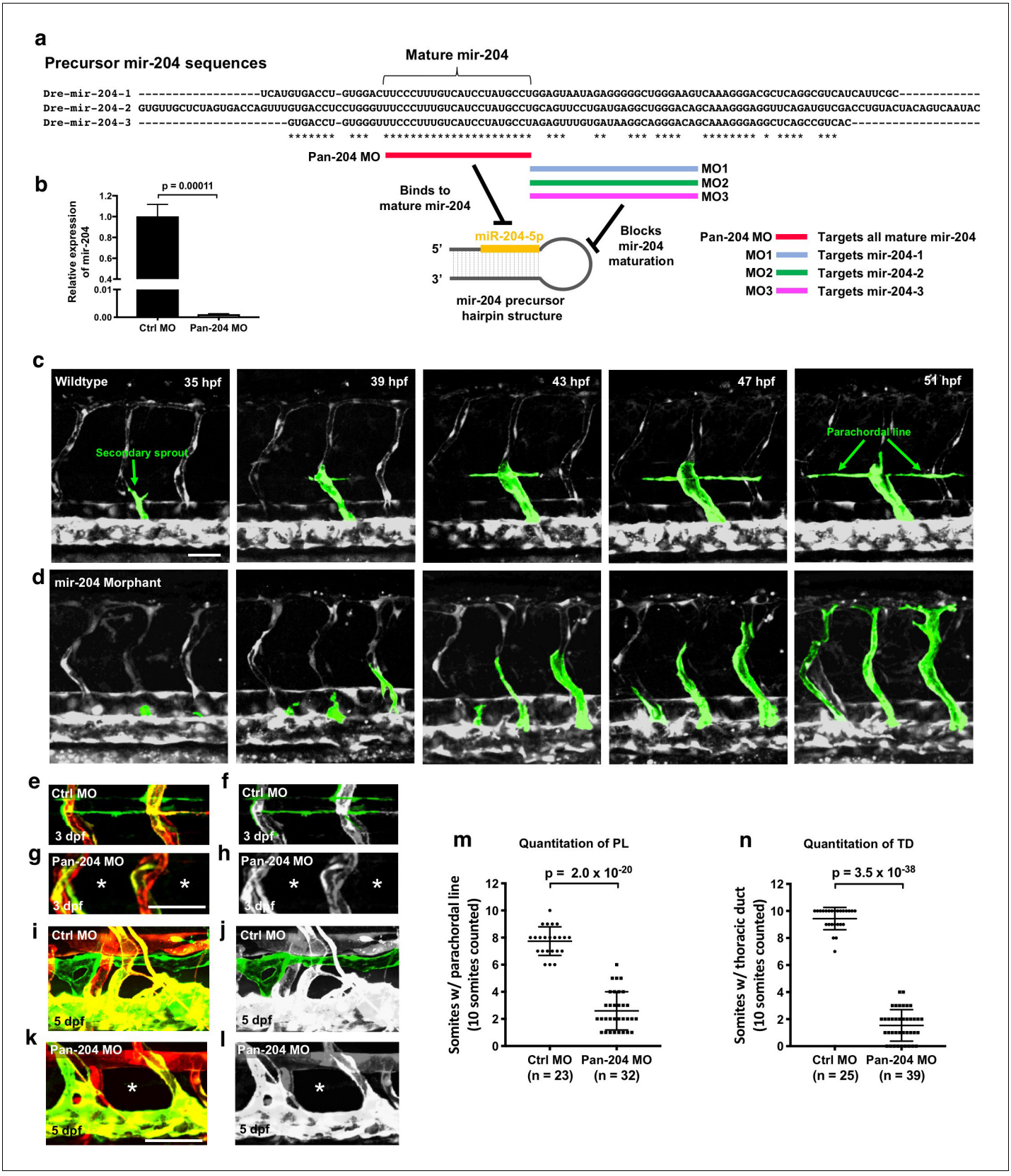

Figure 2. Defective lymphangiogenesis in mir-204 deficient zebrafish. (a) Sequence alignment of the three zebrafish precursor mir-204 sequences (*mir-204–1, mir-204–2,* and *mir-204–3*) and a schematic diagram showing four morpholinos (pan-204 MO, MO1, MO2, and MO3) targeting them. The data

Figure 2 continued on next page

Figure 2 continued

shown in the rest of this figure (panels b-m) uses the pan-204 MO targeting the mature mir-204 sequence generated by all three zebrafish mir-204 loci. (**b**) Quantitative TaqMan RT-PCR measurement of the relative levels of mature miR-204 in one dpf control MO- or pan-204 MO-injected embryos, normalized to controls. Three biological replicates were analyzed. (**c,d**) Time series of confocal images of trunk vessels in 35–51 hpf *Tg(mrc1a:eGFP)*^{y251}*; Tg(kdrl:mCherry)*^{y171} control (**c**) or pan-204 morphant (**d**) animals, with secondary sprouts highlighted in green. (**e–h**) Confocal images of the parachordal line in three dpf *Tg(mrc1a:eGFP)*^{y251}*;Tg(kdrl:mCherry)*^{y171} animals injected with either control MO (**e, f**) or pan-204 MO (**g, h**). In panel f the parachordal line is highlighted in green and other vessels are in gray. The absence of the parachordal line is noted with asterisks in panels g and h. (**i–l**) Confocal images of the thoracic duct in five dpf *Tg(mrc1a:eGFP)*^{y251}*;Tg(kdrl:mCherry)*^{y171} animals injected with either control MO (**i, j**) or pan-204 MO (**k, l**). In panel j the thoracic duct is highlighted in green and other vessels are in gray. The absence of the thoracic duct is noted with asterisks in panels k and l. (**m**) Quantification of parachordal line formation in three dpf animals injected with either control MO (n = 23) or pan-204 MO (n = 32). The same 10 somitic segments were scored in each animal for the presence or absence of an intact parachordal line. (**n**) Quantification of thoracic duct formation in five dpf animals injected with either control MO (n = 25) or pan-204 MO (n = 39). The same 10 somitic segments were scored in each animal for the presence or absence of an intact thoracic duct. All images are lateral views. Scale bar: 50 μm (**c, g, k**). All graphs are analyzed by t-test and the mean ± SD is shown.

DOI: https://doi.org/10.7554/eLife.46007.007

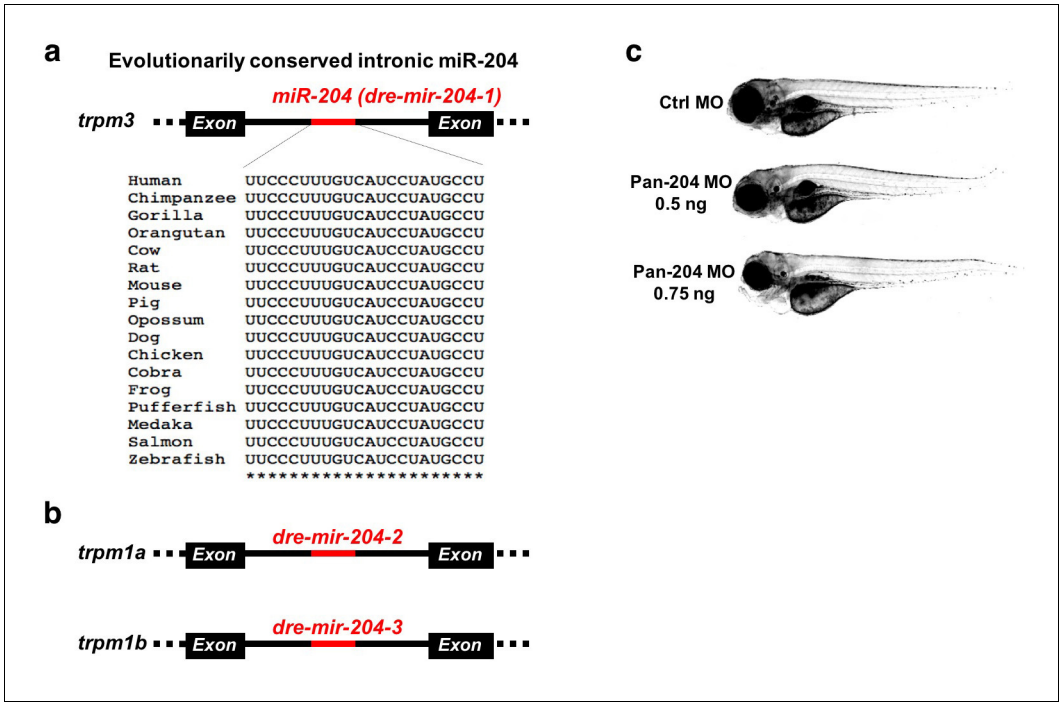

Figure 2—figure supplement 1. Evolutionarily conservation of miR-204. (**a**) Schematic diagram showing the location of miR-204 in intronic region of TRPM3 gene and the 100% conservation of its mature microRNA sequence amongst various vertebrate species. (**b**) Schematic of two additional zebrafish mir-204 loci located in intron 5 and 4 of *trpm1a* and *trpm1b*, respectively. (**c**) Bright field microscopic images of 5 dpf zebrafish larve that were injected with 0.5 ng of control MO (top) 0.5 ng of pan-204 MO (middle), or 0.75 ng of pan-204 MO (bottom).
DOI: https://doi.org/10.7554/eLife.46007.008

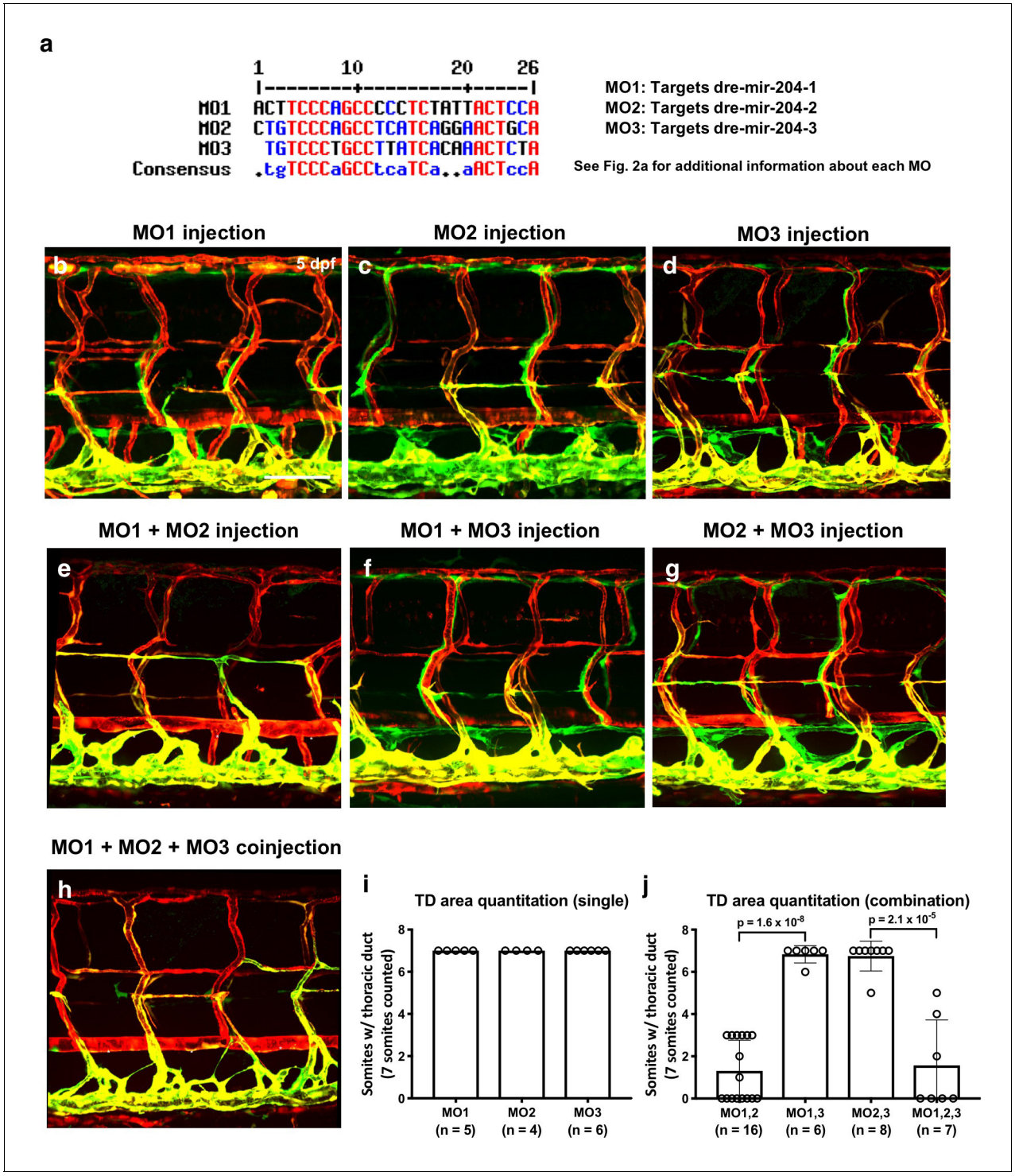

Figure 2—figure supplement 2. The effects of single or combined injections of mir-204 targeting MOs. (**a**) Sequence alignment of MO1, 2, 3. (**b-h**) Representative confocal images of 5 dpf *Tg(mrc1a:eGFP)*^{y251}, *Tg(kdrl:mCherry)*^{y171} double-transgenic animals injected with 0.5 ng of MO1 (**b**), MO2 (**c**), or MO3 (**d**); injected pairwise with 0.5 ng each of MO1+MO2 (**e**), MO1+MO3 (**f**), or MO2+MO3 (**g**), for a final combined MO dose of 1.0 ng in each case; injected with 0.5 ng each of MO1+MO2+MO3 (**h**), for a final combined MO dose of 1.5 ng. (**i**) Quantitation of the single MO injections in panels b-d. (**j**) Quantitation of the combined MO injections in panels e-h. All images are lateral views, rostral to the left. Scale bar: 100 μm (b). All graphs are analyzed by t-test and the mean ± SD is shown.

DOI: https://doi.org/10.7554/eLife.46007.009

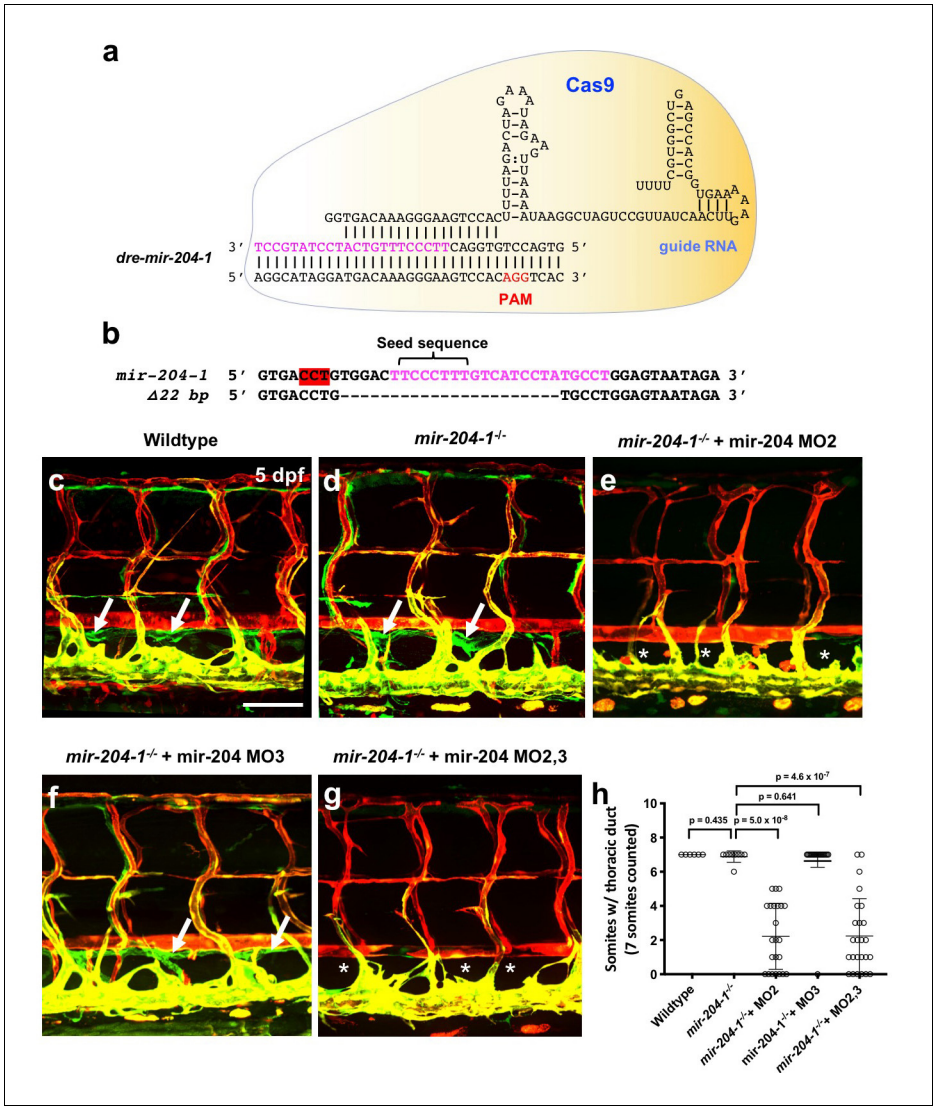

Figure 3. Mir-204 function is required for lymphatic development. (**a**) Schematic of CRISPR/Cas9 and guide RNA targeting of *mir-204–1*. (**b**) Sequence alignment of wildtype and *mir-204–1* mutant genomic DNA. The mature mir-204 sequence is noted in magenta, and the PAM sequence is highlighted in red (on the reverse strand). The mutant carries 22 bp deletion that removes 17 nucleotides of the mature mir-204 sequence. (**c–g**) Representative confocal images of the mid-trunk of 5 dpf wild type sibling (**c**), *mir-204–1*$^{-/-}$ mutant (**d**), MO2-injected *mir-204–1*$^{-/-}$ mutant (**e**), MO3-injected *mir-204–1*$^{-/-}$ mutant (**f**), and MO2 + MO3 co-injected *mir-204–1*$^{-/-}$ mutant (**g**) animals. Images are lateral views of *Tg(mrc1a:eGFP)*^{y251}, *Tg(kdrl:mCherry)*^{y171} double-transgenic animals, rostral to the left. The thoracic duct is labeled with white arrows, and absence of the thoracic duct is noted with asterisks. (**h**) Quantification of thoracic duct formation in five dpf wild type (n = 6), *mir-204–1*$^{-/-}$ mutant (n = 9), MO2-injected *mir-204–1*$^{-/-}$ mutant (n = 23), MO2-injected *mir-204–1*$^{-/-}$ mutant (n = 19), and MO2 + MO3 co-injected *mir-204–1*$^{-/-}$ mutant animals (n = 25). The number of somitic segments with an intact thoracic duct was counted, with the same seven mid-trunk somites measured in each animal. Scale bar: 100 μm (**c**). All graphs are analyzed by t-test and the mean ± SD is shown.

DOI: https://doi.org/10.7554/eLife.46007.012

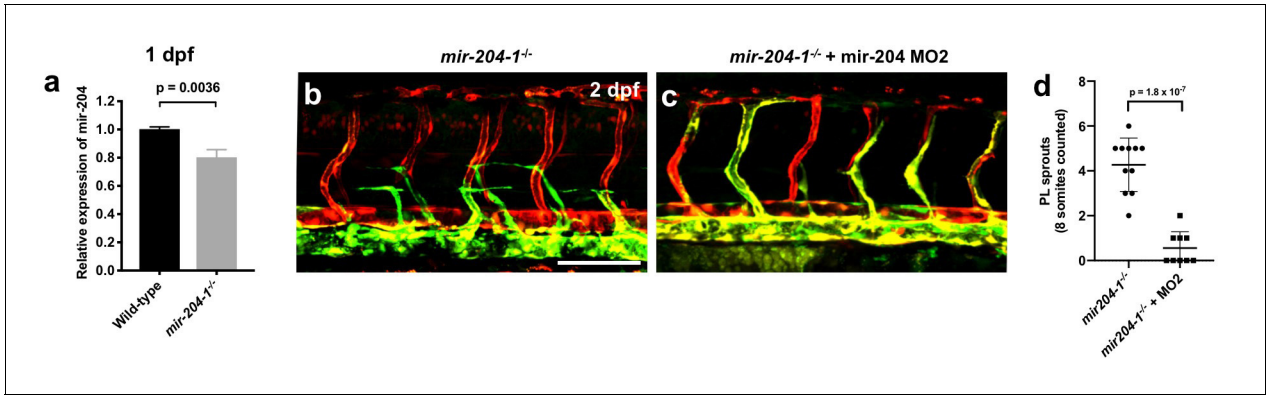

Figure 3—figure supplement 1. Lymphatic differentiation defects in mir-204-deficient animals. (**a**) Quantitative TaqMan RT-PCR measurement of the relative levels of mature mir-204 in one dpf *mir-204–1*$^{-/-}$ mutants and wildtype siblings, normalized to wild type levels. (**b,c**) Confocal images of 2 dpf *Tg (mrc1a:eGFP)*^{y251}, *Tg(kdrl:mCherry)*^{y171} *mir-204–1*$^{-/-}$ mutant (**c**) or MO2-injected *mir-204–1*$^{-/-}$ mutant (**d**) animals. (**d**) Quantitation of the number of PL sprouts in animals as in panels b and c. Scale bar: 100 μm (**b**). All graphs are analyzed by t-test and the mean ± SD is shown.

DOI: https://doi.org/10.7554/eLife.46007.013

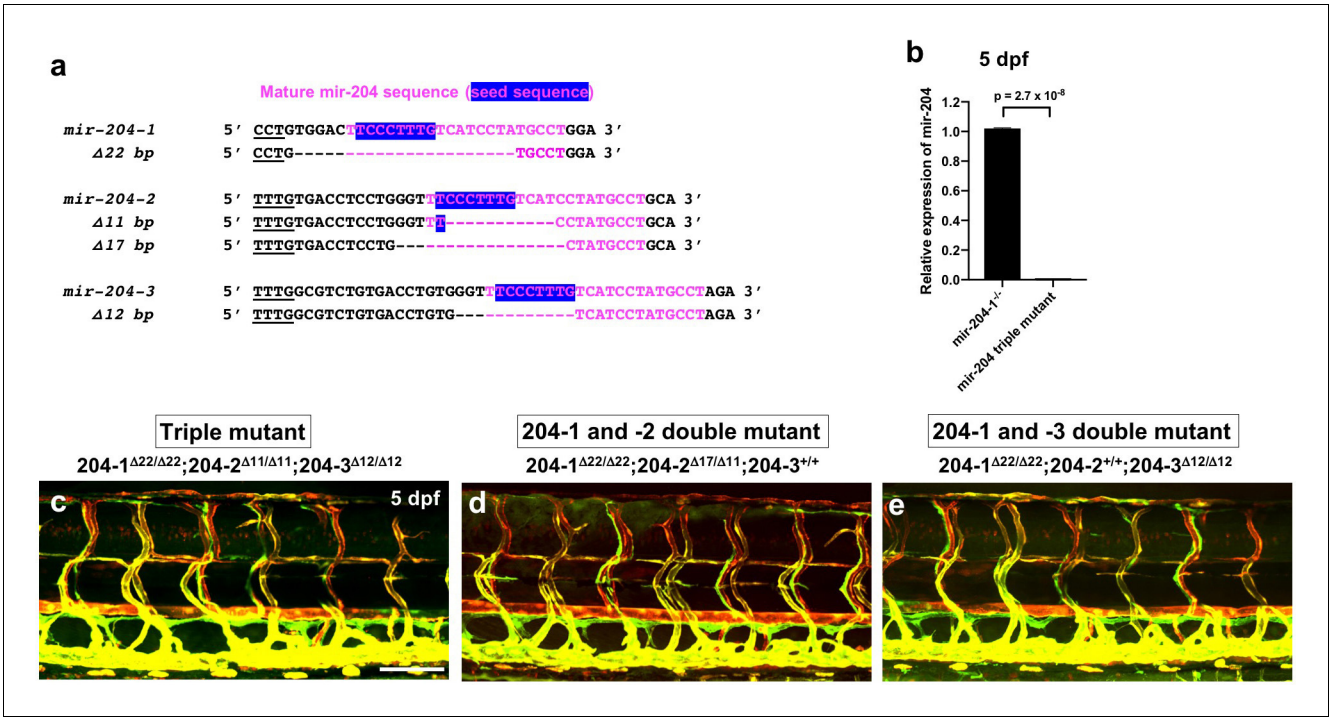

Figure 3—figure supplement 2. MicroRNA 204 mutants. (**a**) Sequence alignment of mir-204–1, −2, and −3 wildtype and deletion mutant. The mature mir-204 sequence are noted with magenta lettering and the seed sequence is highlighted in blue. (**b**) Quantitative TaqMan RT-PCR measurement of the relative levels of mature mir-204 in five dpf *mir-204* triple mutants and their *mir-204–1*$^{-/-}$ siblings, normalized to *mir-204–1*$^{-/-}$ mutants. Three biological replicates were analyzed. (**c–e**) Confocal image of 5 dpf *Tg(mrc1a:eGFP)*^{y251}, *Tg(kdrl:mCherry)*^{y171} mir-204 triple mutant (**c**), *mir-204–1* and *−2* double mutant (**d**), and *mir-204–1* and *−3* double mutant (**e**) animals. All images are lateral views, rostral to the left. Scale bar: 100 μm (**c**). All graphs are analyzed by t-test and the mean ± SD is shown.

DOI: https://doi.org/10.7554/eLife.46007.014

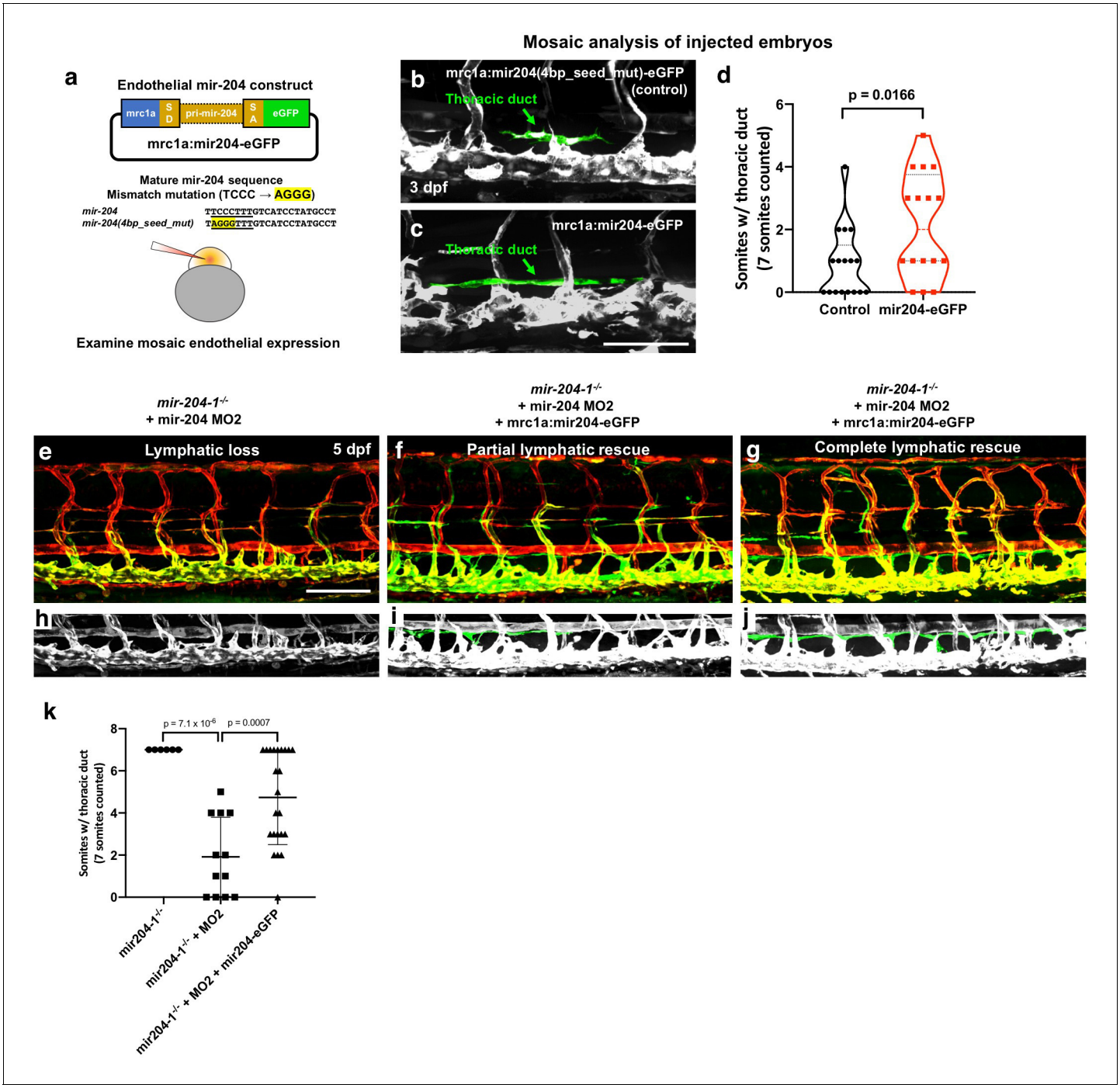

Figure 4. Endothelial expression of mir-204 drives precocious lymphatic development and rescues the loss-of-lymphatic phenotype in mir-204-deficient animals. (**a**) Schematic illustration of the mir-204 expression construct. The EGFP expression cassette is driven by the *mrc1a* promoter (***Jung et al., 2017***), with ~1 kb of *dre-miR-204–1* genomic sequence from the fifth intron of the *trpm3* gene cloned between splice donor (SD) and splice acceptor (SA) sequences and flanking exonic sequences from the *ef1a* gene. The original vector backbone was previously described (***Nicoli et al., 2010***). As a control, a 4 bp mismatch mutation was introduced in the seed (underline) sequence of mature mir-204 sequence. The construct was injected into 1 cell stage embryos to examine the mosaic endothelial expression. (**b,c**) Representative confocal images of mid-trunk of 3 dpf embryos injected with (**b**) control *mrc1a:mir204(4 bp_seed_mut)-eGFP* DNA or (**c**) *mrc1a:mir204-eGFP* DNA. The thoracic duct is pseudocolored in green, with other vessels in gray. (**d**) Quantification of thoracic duct formation in animals injected with either *mrc1a:eGFP* control or *mrc1a:mir204-eGFP* DNA. (**e–g**) Confocal images of *Tg(mrc1a:eGFP)*^{y251}, *Tg(kdrl:mCherry)*^{y171} double-transgenic MO2-injected *mir-204–1*$^{-/-}$ mutant animals without (**e**) or with (**f,g**) co-injected *mrc1a:mir204-eGFP* DNA. (**h–j**) Cropped portions of the corresponding images in e-g, with the thoracic duct pseudocolored in green and other nearby vessels in gray. (**k**) Quantification of thoracic duct formation in animals as in panels e-g. The number of somitic segments with an intact thoracic duct

Figure 4 continued on next page

Figure 4 continued

was counted, with the same seven mid-trunk somites measured in each animal. Scale bar: 100 μm (**c,e**). All graphs are analyzed by t-test and the mean ± SD is shown.

DOI: https://doi.org/10.7554/eLife.46007.016

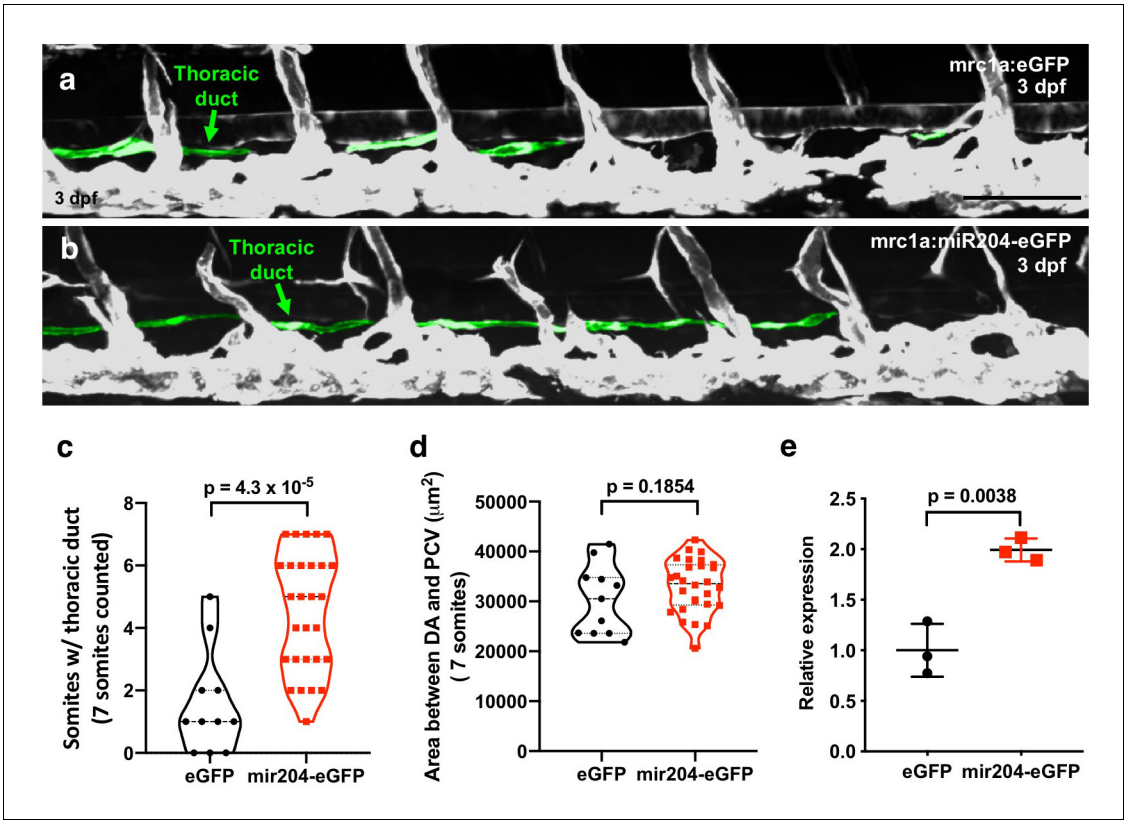

Figure 4—figure supplement 1. Germline endothelial expression of mir-204 drives precocious lymphatic development. (**a**,**b**) Representative confocal images of mid-trunk of 3 dpf of (**a**) *Tg(mrc1a:eGFP)* or (**b**) *Tg(mrc1a:mir204-eGFP)*. The thoracic duct is pseudocolored in green, with other vessels in gray. (**c**) Quantification of thoracic duct formation in animals as in panels a and b. The number of somitic segments with an intact thoracic duct was counted, with the same seven mid-trunk somites measured in each animal. (**d**) Quantification of the area between the dorsal aorta (DA) and posterior cardinal vein (PCV) in animals as in panels a and b, as an indicator of developmental timing. (**e**) Quantitation of mir-204 level measured by TaqMan qPCR from whole embryo at three dpf. All graphs are analyzed by t-test and the mean ± SD is shown.

DOI: https://doi.org/10.7554/eLife.46007.017

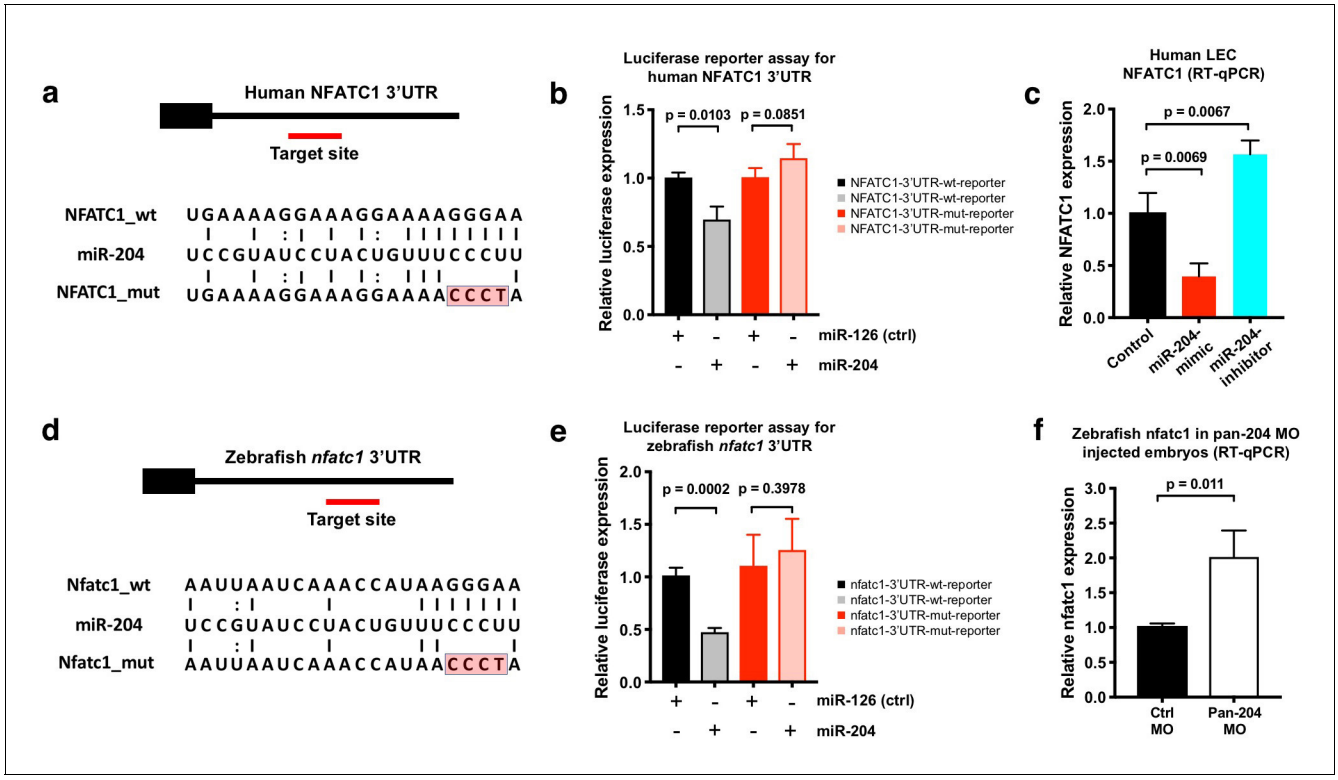

Figure 5. NFATC1 is a conserved target of miR-204. (**a**) Sequence alignment of mature miR-204 (middle line) and its target region in the human NFATC1 3'UTR (top line). A mutant form of the human NFATC1 3'UTR used for the luciferase assay in panel b is also shown (bottom line; four mismatches in the seed binding region are highlighted in red). (**b**) Quantitative luciferase reporter assay using wild type or mutant forms of the human NFATC1 3'UTR transfected into HEK293 cells together with either miR-204 or miR-126 (control). Four biological replicates were analyzed. (**c**) Quantitative TaqMan RT-PCR measurement of relative endogenous NFATC1 transcript levels in human LEC (HMVEC-dLy) transfected with miR-204-mimic or miR-204-antagomir, normalized to control mock transfected levels. (**d**) Sequence alignment of mature miR-204 (middle line) and its target region in the zebrafish nfatc1 3'UTR (top line). A mutant form of the zebrafish nfatc1 3'UTR used for the luciferase assay in panel e is also shown (bottom line; four mismatches in the seed binding region are highlighted in red). (**e**) Quantitative luciferase reporter assay using wildtype or mutant forms of the zebrafish nfatc1 3'UTR co-transfected into HEK293 cells together with either miR-204 or miR-126 (control). Four biological replicates were analyzed. (**f**) Quantitative TaqMan RT-PCR measurement of relative endogenous zebrafish nfatc1 transcript levels in five dpf animals that were injected with either control MO or pan-204 MO. Three biological replicates were analyzed. All graphs are analyzed by t-test and the mean ± SD is shown.
DOI: https://doi.org/10.7554/eLife.46007.019

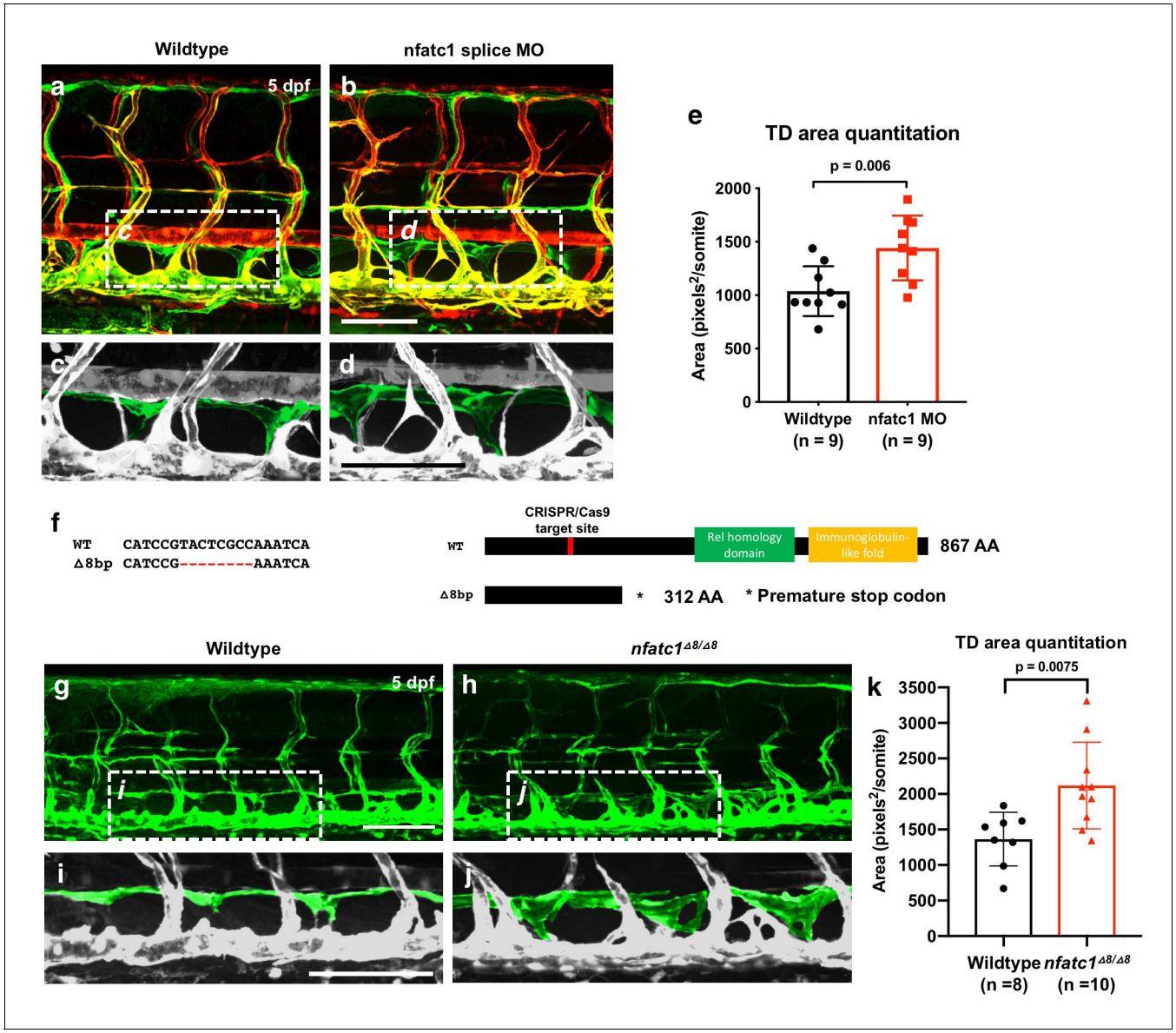

Figure 6. Suppression of Nfatc1 promotes enlargement of the thoracic duct. (**a,b**) Confocal images of the mid-trunk of 5 dpf *Tg(mrc1a:eGFP)*^{y251}, *Tg(kdrl:mCherry)*^{y171} double-transgenic control MO (**a**) or nfatc1 splice MO (**b**) injected animals. The dashed boxes in panels a and b show the areas magnified in panels c and d, respectively. (**c,d**) Magnified images from panels a and b, with the thoracic duct pseudocolored in green and other vessels in gray. (**e**) Quantitation of thoracic duct size measured as the area encompassed by the thoracic duct in confocal images of the same seven mid-trunk somitic segments in five dpf wildtype (n = 9) and nfatc1 MO-injected (n = 9) animals. (**f**) Sequence alignment of wildtype and *nfatc1*$^{\Delta 8/\Delta 8}$ mutant genomic DNA. Schematic of nfatc1 protein domains, CRISPR target site, and truncated mutant nfatc1 polypeptides. (**g,h**) Confocal images of the mid-trunk of 5 dpf *Tg(mrc1a:eGFP)*^{y251} wildtype (**g**) or *nfatc1*$^{\Delta 8/\Delta 8}$ mutant (**h**) animals. (**i,j**) Magnified images from panels g and h, with the thoracic duct pseudocolored in green and other vessels in gray. (**k**) Quantitation of thoracic duct size measured as the area encompassed by the thoracic duct in confocal images of the same seven mid-trunk somitic segments in five dpf wildtype (n = 8) and *nfatc1*$^{\Delta 8/\Delta 8}$ mutant (n = 10) animals. Rostral is to the left in all images. Scale bar = 100 µm (**b,d,g,i**). All graphs are analyzed by t-test and the mean ± SD is shown.

DOI: https://doi.org/10.7554/eLife.46007.021

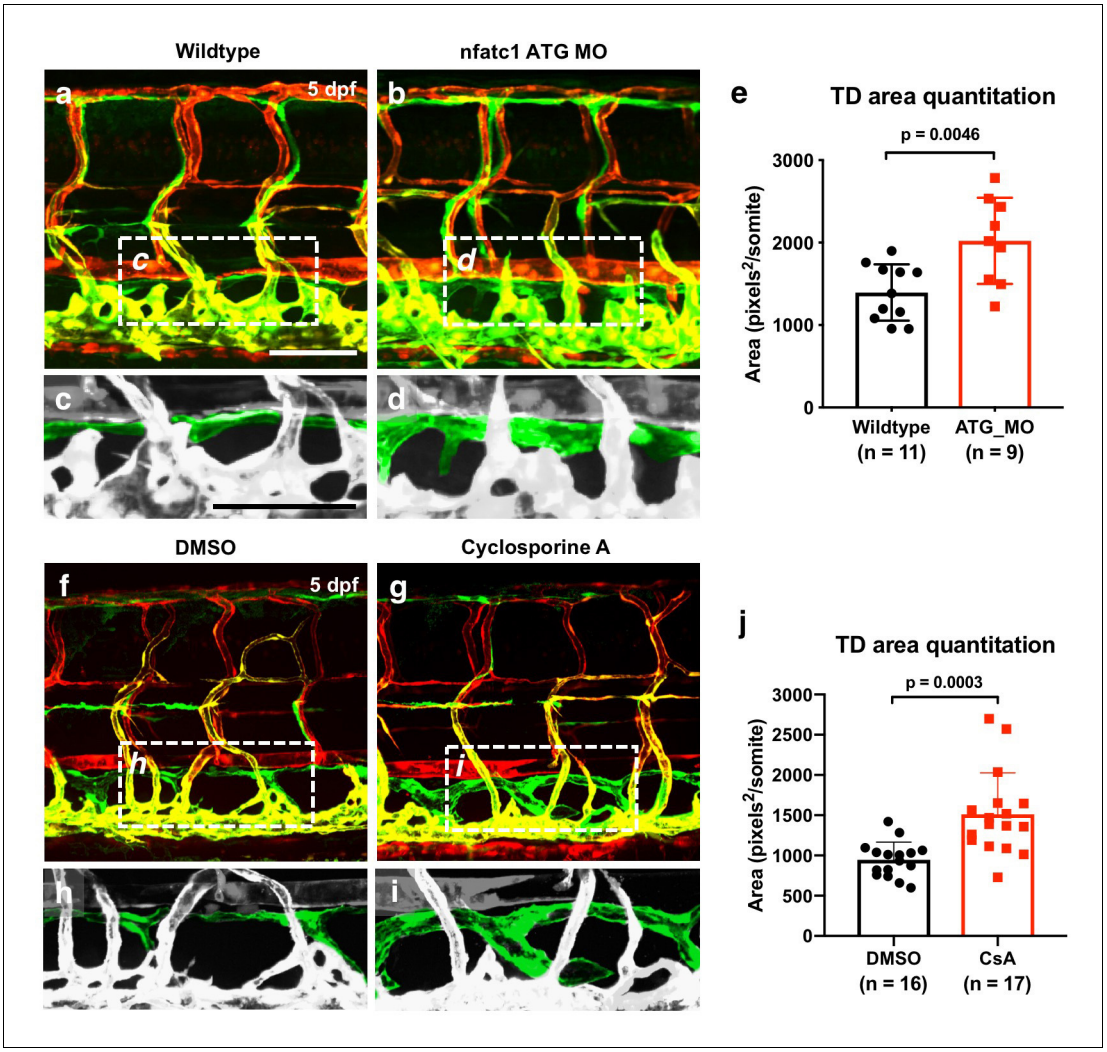

Figure 6—figure supplement 1. Suppressing nfatc1 promotes thoracic duct enlargement. (**a,b**) Confocal images of the mid-trunk of 5 dpf *Tg(mrc1a:eGFP)*^{y251}, *Tg(kdrl:mCherry)*^{y171} control (**a**) and nfatc1 ATG MO-injected (**b**) animals. The dashed boxes in panels a and b show the areas magnified in panels c and d, respectively. (**c,d**) Magnified images from panels a and b, with the thoracic duct pseudocolored in green and other vessels in gray. (**e**) Quantitation of thoracic duct size measured as the area encompassed by the thoracic duct in confocal images of the same seven mid-trunk somitic segments in five dpf wildtype (n = 11) and nfatc1 MO-injected (n = 9) animals. (**f,g**) Confocal images of the mid-trunk of 5 dpf DMSO (**f**) and cyclosporine A (**g**) treated animals. The dashed boxes in panels f and g show the areas magnified in panels h and i, respectively. (**h,i**) Magnified images from panels f and g, with the thoracic duct pseudocolored in green and other vessels in gray. (**j**) Quantitation of thoracic duct size measured as the area encompassed by the thoracic duct in confocal images of 7 somitic segments from five dpf DMSO (n = 16) and cyclosporine A (n = 17) treated animals. All images are lateral views, rostral to the left. Scale bar: 100 μm (**a,c**). All graphs are analyzed by t-test and the mean ± SD is shown.
DOI: https://doi.org/10.7554/eLife.46007.022

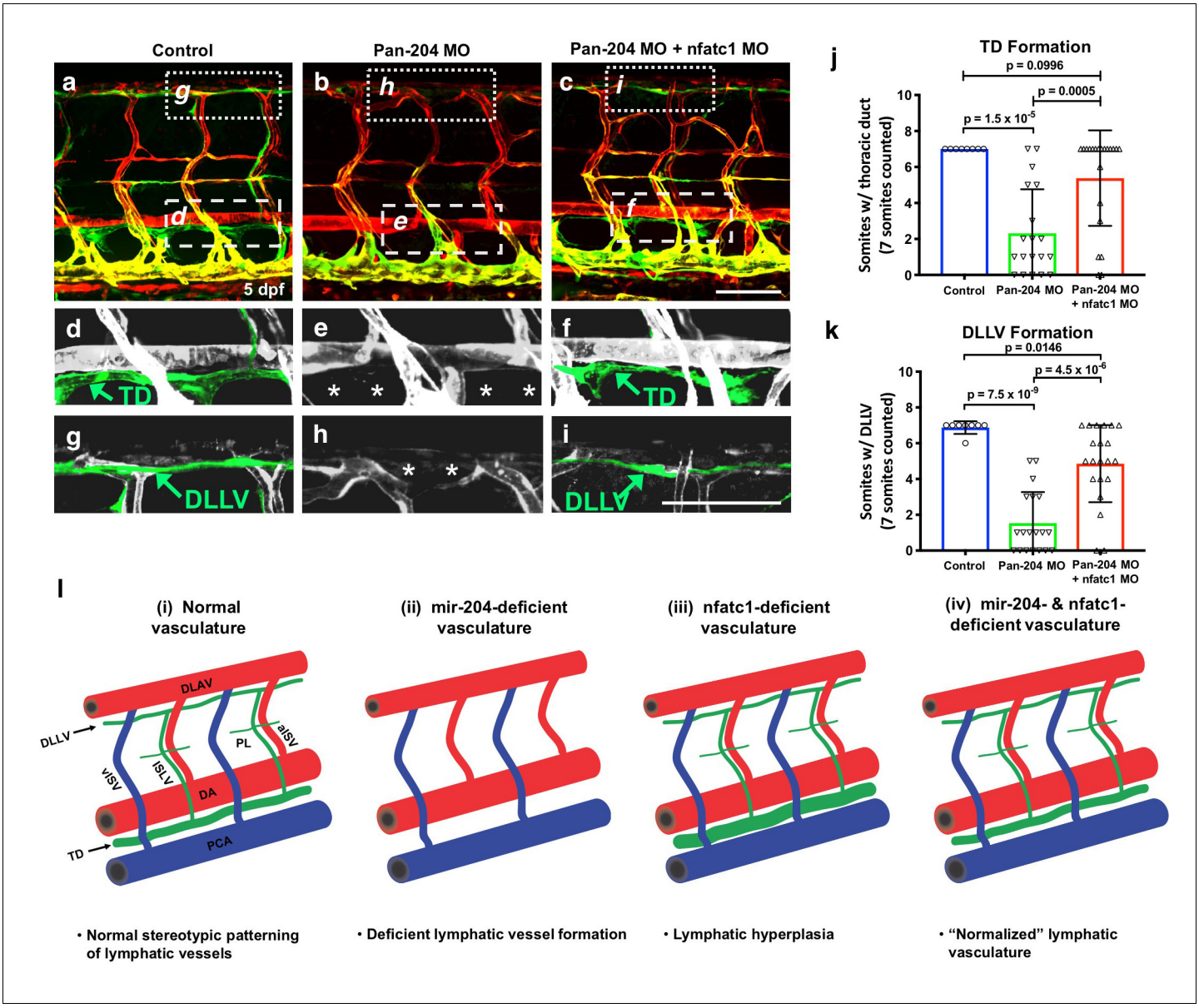

Figure 7. Suppression of nfatc1 rescues the lymphatic defects in mir-204-deficient animals. (**a–c**) Confocal images of the mid-trunk of 5 dpf control (**a**) pan-204 MO-injected (**b**) or pan-204 MO and nfatc1 splice MO co-injected (**c**) animals. White dotted boxes in panels a-c show areas magnified in panels d-f, respectively, while white dashed boxes show areas magnified in panels g-i, respectively. (**d–f**) Magnified images from panels a-c with the thoracic duct (TD) pseudocolored in green and other vessels in gray. The TD is labeled, and the absence of the TD is noted with asterisks. (**g–i**) Magnified images from panels a-c with the dorsal longitudinal lymphatic vessel (DLLV) pseudocolored in green and other vessels in gray. The DLLV is labeled, and the absence of the DLLV is noted with asterisks. (**j**) Quantification of thoracic duct (TD) formation in five dpf control (n = 8), pan-204 MO-injected (n = 19), or pan-204 MO and nfatc1 splice MO co-injected animals (n = 21). A total of 7 mid-trunk somitic segments were scored in each animal for the presence or absence of an intact TD. (**k**) Quantification of dorsal longitudinal lymphatic vessel (DLLV) formation in five dpf control (n = 8), pan-204 MO-injected (n = 19), or pan-204 MO and nfatc1 splice MO co-injected animals (n = 21). A total of 7 mid-trunk somitic segments were scored in each animal for the presence or absence of an intact DLLV. (**l**) Schematic diagrams illustrating five dpf zebrafish trunk lymphatic vessels present in (**i**) normal control, (ii) mir-204 deficient, (iii) nfatc1-deficient, and (iv) mir-204- and nfatc1-deficient animals. Suppression of mir-204 leads to loss of lymphatic vessels (ii), while nfatc1 deficiency causes lymphatic (thoracic duct) hyperplasia (iii). The lymphatic defects in mir-204 deficient animals can be rescued by simultaneous suppression of nfatc1 (iv). All images are lateral views of *Tg(mrc1a:eGFP)*^{y251}, *Tg(kdrl:mCherry)*^{y171} double-transgenic animals, rostral to the left. Scale bar = 100 μm (**c,i**). All graphs are analyzed by t-test and the mean ± SD is shown.

DOI: https://doi.org/10.7554/eLife.46007.024